Experimental Investigation of Near-Field Aeroacoustic Characteristics of a Pre- and Post-Stall NACA 65-410 Airfoil

B. Zang[1]; Yannick D. Mayer[2]; and Mahdi Azarpeyvand[3]

Abstract: The present study reports an experimental investigation of the near-field aeroacoustic characteristics of a cambered NACA 65-410 airfoil. The experiments were performed in an aeroacoustic wind tunnel facility at a moderate chord-based Reynolds number of 4.2×10^5. Detailed static and dynamic surface pressure information was recorded to reveal the pre- and post-stall dynamics. By varying the angle of attack from 7° to 15°, a stall behavior similar to thin airfoil stall is observed from the evolution of the static and dynamic surface pressure spectra at different chordwise locations. Moreover, while the surface pressure spectra show a monotonic decrease with constant gradients after entering full stall, the pre-stall behavior shows a different trend and partly resembles the attached and stalled flows. Furthermore, the unsteady surface pressure spectra are compared to those obtained from a NACA 0012 airfoil, showing notable differences in the near-field stall dynamics. A scaling formula proposed by a previous study is applied to the present pressure spectra and found to scale well except for measurements close to the leading edge. The present near-field measurements and the streamwise and spanwise length scales can be useful input to the modeling of airfoil separation and stall noise for cambered airfoils. **DOI: 10.1061/(ASCE)AS.1943-5525.0001318.** © *2021 American Society of Civil Engineers.*

Introduction

Airfoil stall noise is an important aspect of airfoil self-noise, and can potentially be a major contributor to environmental noise—for instance, when wind turbines are operated at pre-stall and even post-stall conditions. Airfoil stall noise is generated through the interaction between the turbulent structures in the separated shear layer with the airfoil surface, as these structures are convected past the airfoil, resulting in significant surface pressure fluctuations (Brooks et al. 1989). The aerodynamic and aeroacoustic characteristics of a stalled airfoil are much less studied than attached flow conditions, because most engineering designs tend to focus on airfoils operating well below the stall angle of attack to prevent undesirable effects, e.g., loss of lift and drastic increase in drag. Nevertheless, pre- and post-stall aerodynamics and aeroacoustics can be of immense interest to engineering applications such as wind turbines, rotors, and turbojet engines (Petrilli et al. 2013), where the airfoils are susceptible to changing inflow conditions. Moreover, when an airfoil is stalled, its self-noise, i.e. stall noise, increases significantly, making it not only detrimental to public health but also a primary hindrance to the large-scale deployment of wind farms for renewable energy harvesting (Moreau et al. 2009).

Early experimental and numerical studies of stall aerodynamics include those from Jones (1934), Mccullough and Gault (1951), and Reilly (1967). Yet, research into airfoil self-noise with separated or stalled flow conditions remained very much limited until the 1970s (Kurtz and Marte 1970). Brooks et al. (1989) conducted the first systematic study of airfoil self-noise, from trailing-edge noise to separation and stall noise. Building upon the measurements of several NACA 0012 airfoils, Brooks et al. (1989) proposed a semi-empirical noise prediction model for airfoil self-noise, known as the Brooks, Pope, and Marcolini (BPM) model. They argued that the model can be applied to other airfoil profiles, assuming the profiles have similar boundary layer properties. However, flow properties and the associated noise generation mechanisms vary notably for heavily loaded airfoils (Moreau et al. 2008). In the case of airfoil stall, the characteristics of the flow separation, i.e. the stall type, are dependent on the airfoil Reynolds number and profile shape, among others. Moreau et al. (2009) conducted experimental and numerical studies of the stall noise of a NACA 0012 airfoil at a relatively low Reynolds number. Employing simultaneous measurements of the surface pressure fluctuation and far-field noise spectrum, they developed a simplified model for predicting stall noise. Later, Schuele and Rossignol (2013) performed aeroacoustic measurements of a partially stalled DU-96-W-180 airfoil, and also derived a stall noise model based on trailing-edge noise theory. More recently, Bertagnolio et al. (2015) experimentally investigated the surface pressure fluctuation spectra of several different airfoils, including NACA 0015 and NACA 63-418 airfoils in pre- and post-stall conditions with Reynolds numbers ranging from 1.6 M to 6 M. Moreover, they attempted to scale the pressure spectra along the chordwise locations with varying Reynolds number, such that it can serve as an input to the accurate modeling of stall noise. Extending this work, Bertagnolio et al. (2017) subsequently presented more comprehensive surface pressure measurements and proposed a stall noise prediction model based on their surface pressure spectra scaling.

Several high-order accurate numerical studies on stall noise have also emerged, such as Moreau et al. (2008), Wolf and Lele (2012), Kocheemoolayil and Lele (2016), and Turner and Kim (2020a, 2020b). Moreau et al. (2008) performed large-eddy simulations (LES) on a NACA 0012 airfoil at post-stall angles of attack of 16° and 18° and found extraneous sound sources at low frequencies. Turner and Kim (2020b) attributed the low-frequency increase

[1]Lecturer, Faculty of Engineering, Univ. of Bristol, Bristol BS8 1TR, UK (corresponding author). ORCID: https://orcid.org/0000-0003-4476-8321. Email: nick.zang@bristol.ac.uk

[2]Honorary Research Associate, Faculty of Engineering, Univ. of Bristol, Bristol BS8 1TR, UK. Email: yannick.mayer@bristol.ac.uk

[3]Professor of Aerodynamics and Aeroacoustics, Faculty of Engineering, Univ. of Bristol, Bristol BS8 1TR, UK. Email: m.azarpeyvand@bristol.ac.uk

Note. This manuscript was submitted on December 2, 2020; approved on April 27, 2021; published online on August 4, 2021. Discussion period open until January 4, 2022; separate discussions must be submitted for individual papers. This paper is part of the ***Journal of Aerospace Engineering***, © ASCE, ISSN 0893-1321.

to the shear layer structures scattering at the trailing edge, while the increase at medium to high frequencies remains unresolved. Indeed, as remarked by Turner and Kim (2020a), the existing literature on stall noise are underdeveloped, and more importantly, the generation mechanisms of airfoil stall noise are underexplained. This demands further research efforts to better understand airfoil stall noise, and ultimately to develop control and mitigation strategies, especially because noise emission regulations are becoming growingly stringent (Jarup et al. 2005; Nobbs et al. 2012).

The present experimental study is inspired by the need to better understand and more accurately model airfoil stall noise, particularly for different airfoil profiles and Reynolds numbers. By experimentally measuring the near-field aeroacoustic characteristics of a cambered NACA 65-410 airfoil at a moderate Reynolds number, the study aims to provide a more comprehensive knowledge of surface pressure fluctuation spectra and correlation length scales at this flow regime, when the angle of attack is varied from pre- to post-stall, i.e., partial flow separation to full stall. Subsequently, the study compares the results with those obtained from a NACA 0012 airfoil in the same facility at similar flow conditions to highlight the different behaviors of the unsteady aerodynamic loading during stall. Furthermore, with the knowledge of the unsteady surface pressure along the airfoil chord, the scaling approach proposed by Bertagnolio et al. (2015) for airfoils undergoing separation and stall is applied to examine the effectiveness of the pressure spectra scaling for the cambered airfoil profile. The presented near-field aeroacoustic results can serve as useful inputs for the modeling of airfoil separation and stall noise. In the following sections, the experimental setup and the airfoil model are briefly introduced. Subsequently, the experimental measurements of the surface pressure fluctuation spectra and correlation length scales are presented to characterize the NACA 65-410 airfoil at pre- and post-stall conditions and compare the results to those of a NACA 0012 airfoil.

Experimental Methodology

All experimental measurements of the NACA 65-410 airfoil have been carried out in the aeroacoustic wind tunnel facility of the University of Bristol. Because the detailed design and the characterization of the flow uniformity and turbulence level have been reported by Mayer et al. (2019a), only a brief summary of the wind tunnel facility is provided here. As shown in Fig. 1, the hybrid closed-circuit open-jet tunnel has a 8.4:1 contraction ratio nozzle, measuring $0.775\,\mathrm{m} \times 0.5\,\mathrm{m}$ at the nozzle exit. The free-stream turbulence intensity at $U_\infty = 20\,\mathrm{m/s}$ is approximately 0.2% without low-frequency filtering. A Kevlar-walled test section is mounted securely to the nozzle exit to house the NACA 65-410 airfoil. The tensioned Kevlar walls at the top and bottom allow airfoil aeroacoustic measurements at high, i.e., post-stall, angles of attack without significant angle-of-attack corrections for sufficiently small chord length. Interested readers are advised to refer to Mayer et al. (2020) for more discussion on the transmission loss and aerodynamic corrections of the test section. The airfoil is located approximately one airfoil chord, $c = 300$ mm, away from the nozzle exit, and aligned at the center of the nozzle to ensure uniform flow past the airfoil.

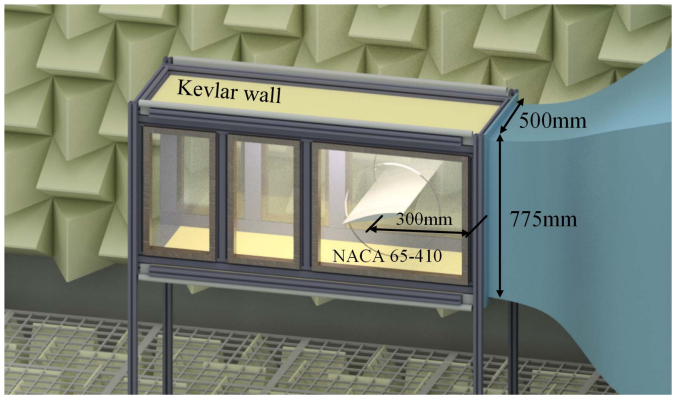

Fig. 1. 3D schematic of the aeroacoustic wind tunnel facility and the Kevlar-walled test section of the present experimental setup.

The NACA 65-410 airfoil used in the present study represents a family of highly cambered thin airfoil profiles, which is often considered a viable starting point for design of turbine blades (Westphal and Godwin 1951). Also, unlike the classic symmetric NACA profiles such as NACA 0012 and NACA 0015, there are fewer experimental characterizations of cambered airfoil profiles. The present 300-mm-chord NACA 65-410 airfoil is machined from aluminum with a hollow inside to accommodate both the static pressure ports and dynamic pressure transducers. As shown in Fig. 2, the static pressure ports, for collecting the static pressure information, are distributed in the chordwise direction along the centerline on the suction and pressure sides of the airfoil (slightly offset from the dynamic transducers), while the dynamic transducers are distributed in chordwise and spanwise directions in order to capture both the streamwise and spanwise flow correlation length scales. The dynamic transducers are primarily located on the suction side to provide a fine resolution of the dynamic events and the associated flow structures. There are two types of dynamic pressure transducers installed in the airfoil: direct-sensing transducers with Knowles FG-23629-P16 condenser microphones (Digi-Key Electronics, Thief River Falls, MN), and, where the space is more limited toward the trailing-edge of the airfoil, remote-sensing transducers with Panasonic WM-61A microphones (Panasonic, Osaka, Japan). All these dynamic pressure transducers were calibrated against a G.R.A.S. 40PL free-field microphone (GRAS, Holte, Denmark) with known sensitivity to determine the sensitivity and phase-transfer functions prior to the experiments. The working principle, calibration, and limitations of the dynamic transducers have been discussed in greater detail in Mish (2003), Szöke (2019), and Vemuri et al. (2020). To eliminate possible tonal noise from Tollmien-Schlichting instabilities and ensure a turbulent boundary layer over the trailing edge of the airfoil at pre-stall angles of attack, zigzag turbulators of 6-mm width were applied to both the suction and pressure sides of the airfoil at approximately 12% of the chord, similar to those used by Lyon et al. (1997) and Garcia-Sagrado (2008).

Experiment and Post-Processing Parameters

The airfoil was tested at a constant free-stream velocity of $U_\infty = 20\,\mathrm{ms}^{-1}$, corresponding to $Re_c = 4.2 \times 10^5$ based on the length of the airfoil chord. In order to carry out correlation and coherence analyses of the unsteady surface pressure between different dynamic transducers, all signals from the 56 dynamic transducers were collected simultaneously by National Instruments PXIe-4499 sound acquisition modules (National Instruments, Austin, Texas) at a sampling rate of 2^{15} Hz. The data were then post-processed with the calibration transfer functions to obtain the calibrated pressure fluctuation time series, and subsequently transformed into the frequency domain via Welch's method (Welch 1967), using a Hamming window size of 2^{13} with a 50% window overlap to obtain the power spectral density (PSD) of the surface pressure fluctuations,

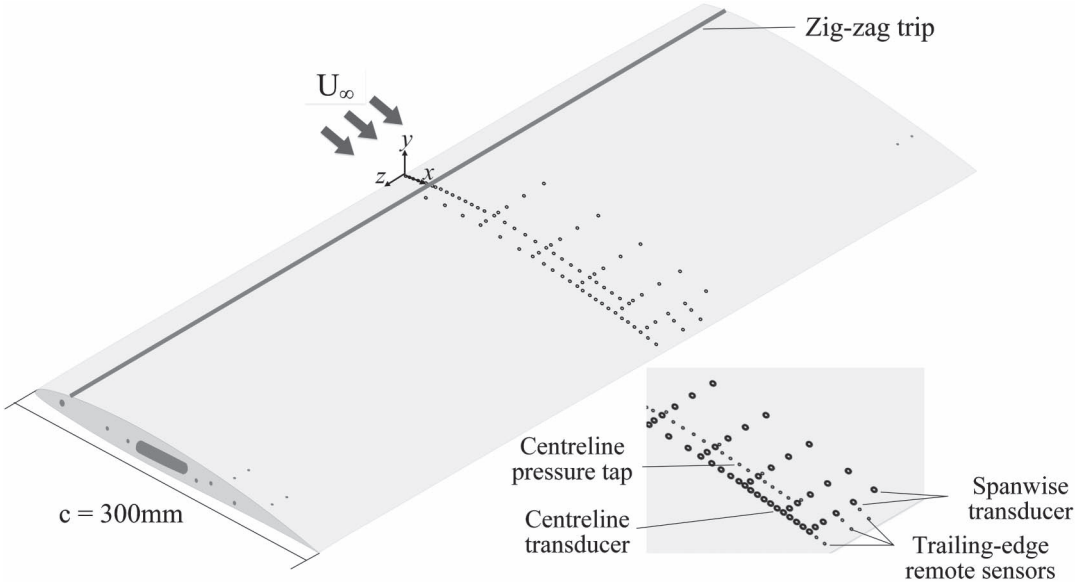

Fig. 2. Instrumented NACA 65-410 airfoil model with zoomed-in view of distribution of the suction side pressure taps and dynamic pressure transducers.

ϕ_{pp}. The resulting pressure fluctuation PSD has a resolution of $\Delta f = 2^3$ Hz and an uncertainty of approximately ± 1.5 Hz/dB at 95% confidence level (Afshari et al. 2019). For the static pressure measurements, the data from the static pressure taps were registered by two MicroDaq-32-DTC pressure scanners at 1,000 Hz for a duration of 60 s, and time-averaged to obtain the mean pressure coefficient (C_p) distributions over the airfoil. The sampling rate of the pressure scanners was chosen such that it complies with the maximum sampling frequency for obtaining accurate measurements with sufficiently large sample size.

Results and Discussion

To investigate the changes of the near-field aeroacoustic characteristics of the NACA 65-410 airfoil from pre- to post-stall flow conditions, the angle of attack is systematically varied through $\alpha = 7°$–$15°$ to gain a complete picture of its stall behavior. It is determined that under the present experimental conditions, the NACA 65-410 airfoil experiences full stall at a geometric angle of attack of $\alpha = 12°$. Subsequently, four distinct angles of attack, $\alpha = 7°$, 10°, 13°, and 15°, have been selected to perform the study, which correspond to pre-, near-, full- and deep-stall conditions. It should also be mentioned that the experimental measurements on NACA 0012 have been carried out previously at a similar Reynolds number, with a more comprehensive range of angles of attack surveyed. Based on the stall behavior, two angles of attack, $\alpha = 15°$ and 18°, will be used correspondingly to represent the full- and deep-stall scenarios for comparison in the following section. Further details of the NACA 0012 experiments can be found in Mayer et al. (2019b, 2020).

Static Surface Pressure Distribution

Before going into the surface pressure fluctuation spectra results, it is useful to first examine the steady aerodynamic behavior of the airfoil from the time-averaged pressure distributions. Fig. 3 shows the time-averaged pressure distributions of the NACA 65-410 airfoil at the four chosen angles of attack. The good agreement

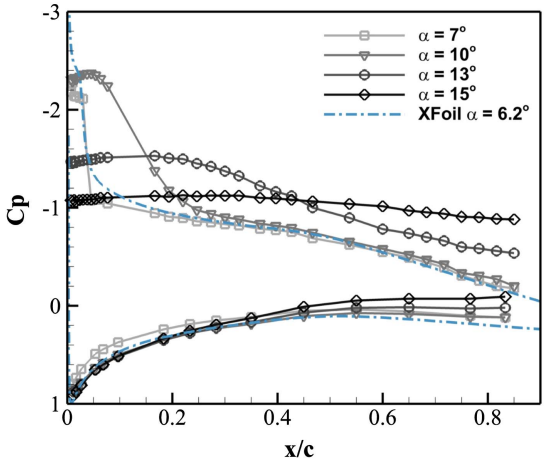

Fig. 3. Time-averaged static pressure distribution (C_p) of the NACA 65-410 at pre- and post-stall angles of attack of $\alpha = 7°$, 10°, 13°, and 15°.

between the C_p distribution at $\alpha = 7°$ and the results from the XFOIL (Drela 1989) simulation at $\alpha = 6.2°$, which is superimposed onto the experimental data in the figure, suggests a minor angle of attack correction from the present setup. It should be remarked that the difference between the XFOIL simulation and the experimental results may partly be attributed to the edge effects of the airfoil, which produce spanwise flow variations along the airfoil surface, resulting in the reduction of the effective angle of attack. Nevertheless, as a stalled airfoil can be identified clearly from both its static pressure distribution and unsteady surface pressure fluctuation spectra along the airfoil chord, the results analysis and discussion hereafter will adhere to the geometric angle of attack. A closer examination of the C_p distribution shows that the airfoil is indeed fully stalled at $\alpha = 13°$ and 15° when the C_p distribution along the suction side is largely flat. However, at $\alpha = 10°$, the C_p distribution undergoes a gradual increase from $x/c = 0.1$ to 0.2, different from either the sharp increase at $\alpha = 7°$ or the plateau

at $\alpha = 13°$. Therefore, from the time-averaged static pressure distribution, it is suspected that partial flow separation takes place on the suction side of the airfoil at $\alpha = 10°$ near the leading edge. By comparing the changes of the static pressure coefficients over increasing angle of attack, as shown in Fig. 3, with the experimental investigation on cambered airfoils by Mccullough and Gault (1951) and Gault (1957), the NACA 65-410 airfoil under the present flow condition shows the likely behavior of a thin airfoil stall. For instance, at $\alpha = 10°$, the flow over the airfoil first separates close to the leading edge, with subsequent reattachment at approximately $x/c = 0.2$. As the angle of attack increases, the separation extends over the entire airfoil chord and the airfoil becomes fully stalled. This behavior is in good agreement with the C_p results from Mccullough and Gault (1951) for a double-wedge airfoil undergoing thin airfoil stall.

Dynamics of Surface Pressure Fluctuations

When the vortices in the boundary layer or the separated flow are convected past the airfoil, the dynamic interaction process between the turbulent structures and the airfoil surface induces surface pressure fluctuations. Expectedly, the energy frequency contents of the surface pressure fluctuation ϕ_{pp} increase as the flow separates, with growing turbulent structures originating and developing along the shear layers. Fig. 4 shows the contour variations of the surface pressure fluctuation spectra from $\alpha = 7°$ to $15°$ for the two chordwise locations of $x/c = 0.23$ and 0.65. The reference pressure p_0 is 2×10^{-5} Pa. Also, note that for the sake of brevity, results further downstream of $x/c = 0.65$ are not presented here because these two locations represent the overall behavior of the unsteady surface pressure spectra well. Generally, a notable increase in the low-frequency energy contents ($f \leq 1{,}000$ Hz) of the surface pressure fluctuation spectra can be observed when the airfoil is approaching stall beyond $\alpha = 10°$, indicating the presence of large-scale turbulent structures as the flow over the airfoil suction side separates. This is accompanied by a decrease in the high-frequency energy contents because the smaller turbulent structures are being lifted away from the airfoil surface in the separated flow. Recall that Moreau et al. (2009) and Turner and Kim (2020b) observed a significant increase of far-field noise at low frequencies of approximately below 400 Hz for stalled airfoils; hence, the growth of energy contents at low frequencies in the near-field surface pressure fluctuation correlates well with the elevated noise levels at the low frequencies. Moreover, the increase appears to take place gradually over 2° to 3° of angles of attack, suggesting possibly a flow transition to partial separation before stall. Indeed, such a transition can be clearly observed by comparing the spectra variations with the angle of attack at the two chordwise locations of $x/c = 0.23$ and 0.65, as shown in Figs. 4(a and b) respectively. At $x/c = 0.65$, the notable increase in low-frequency energy contents takes place immediately after approximately $\alpha = 10°$, whereas at $x/c = 0.23$, such an increase appears to first occur between the frequency range of 500 Hz $\leq f \leq$ 1,200 Hz, and subsequently the spectra become comparable to those at $x/c = 0.65$ once the airfoil is fully stalled. Recall from the static pressure distribution in Fig. 3 that at $x/c = 0.23$, the flow undergoes the separation and reattachment process, hence showing noticeably different spectral behavior from those measured at further downstream locations.

Figs. 5 and 6 provide a more direct assessment of the changes in surface pressure fluctuation spectra for eight different chordwise locations from the leading edge to the trailing edge at the four selected angles of attack, $\alpha = 7°$, 10°, 13°, and 15°. Note that in order to discern each spectra clearly, each angle of attack is further divided into two subplots. For $\alpha = 7°$, the surface pressure fluctuation spectra at low frequencies ($f \leq 1{,}000$ Hz) first increase to reach a local maximum before decreasing with a gradient of approximately f^{-1} in the mid frequencies, followed by a faster roll-off of f^{-3} at $f \geq 6{,}000$ Hz. The PSD magnitude increases consistently from the leading edge to the trailing edge. Such developments and dynamics are typical of the surface pressure fluctuation spectra for an attached airfoil flow, similar to those reported by Garcia-Sagrado (2008) and Mayer et al. (2019b) for NACA 0012 airfoils. Thus, it can be seen that the flow remains fully attached to the airfoil at $\alpha = 7°$. Increasing angle of attack to $\alpha = 10°$ will see the spectra increase shortly at the low frequencies of $f \leq 400$ Hz, and then decay with an almost constant gradient of approximately f^{-2}. For post-stall angles of attack, $\alpha = 13°$ and 15°, the surface pressure fluctuation spectra essentially follow a monotonic decrease with a constant gradient of f^{-2} throughout the frequency range investigated. Signs of an accelerated roll-off at high frequencies can be observed toward $f \geq 7{,}000$ Hz. Bertagnolio et al. (2015, 2017) and Mayer et al. (2020) reported similar behaviors of the surface pressure fluctuations when their airfoils entered full stall. However, unlike the symmetric NACA 0015 and NACA 0012 airfoils in their studies, the cambered NACA 65-410 shows a much smaller magnitude fluctuations in the spectra from the leading edge to the trailing edge, agreeing with the results of the NACA 63-418 airfoil by Bertagnolio et al. (2017).

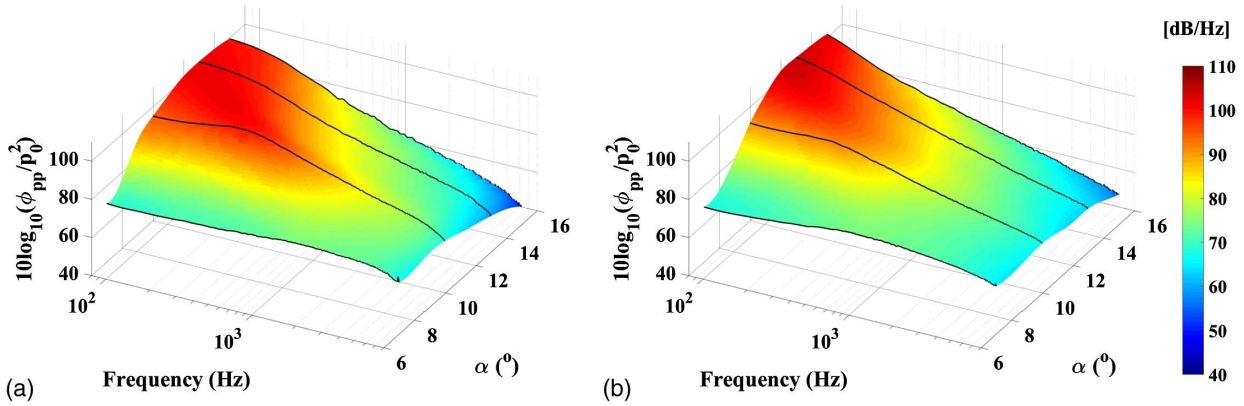

Fig. 4. Contour maps of the unsteady surface pressure spectra from $\alpha = 7°$ to 15° at 1° intervals measured at the chordwise locations of (a) $x/c = 0.23$; and (b) $x/c = 0.65$.

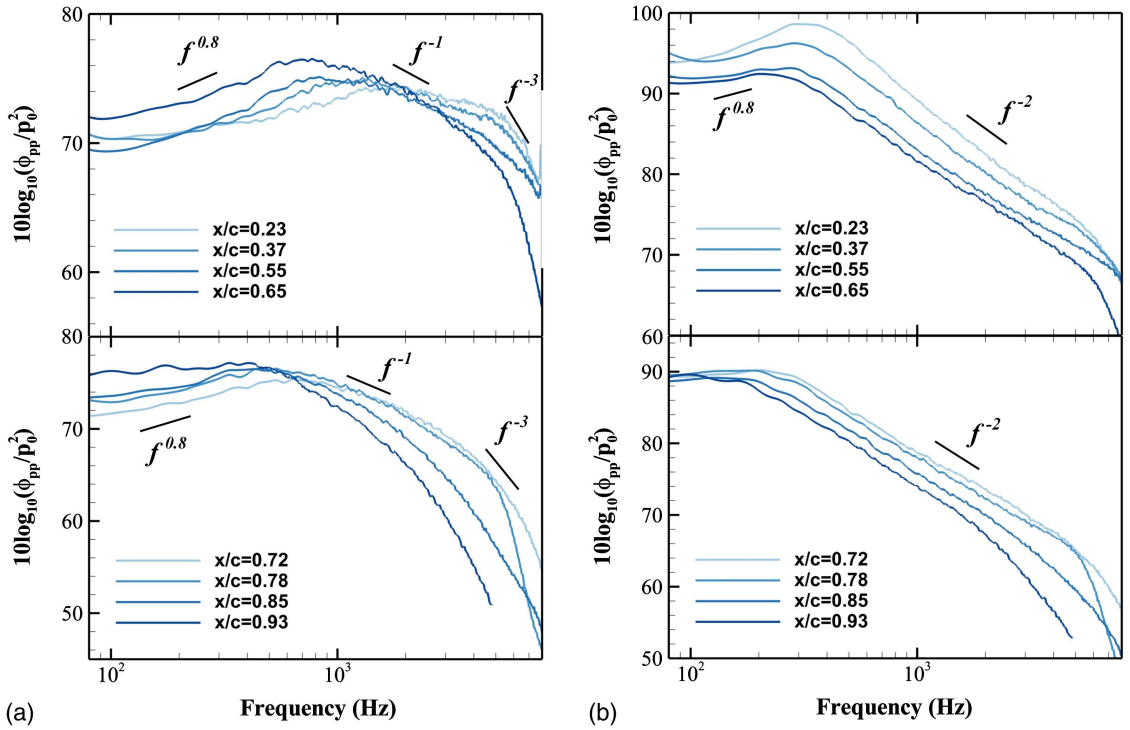

Fig. 5. Power spectral density of the surface pressure fluctuations at eight chordwise locations from the leading edge to the trailing edge of the NACA 65-410 at near-stall angles of attack of (a) $\alpha = 7°$; and (b) $\alpha = 10°$.

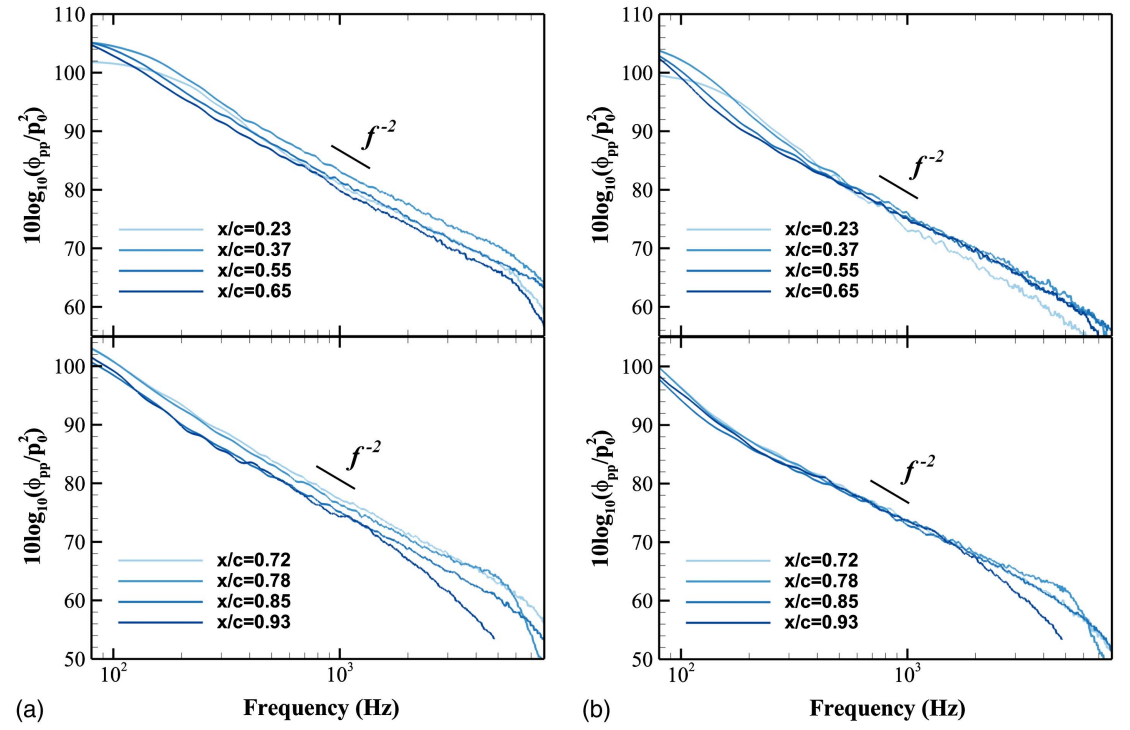

Fig. 6. Power spectral density of the surface pressure fluctuations at eight chordwise locations from the leading edge to the trailing edge of the NACA 65-410 at post-stall angles of attack of (a) $\alpha = 13°$; and (b) $\alpha = 15°$.

Comparison of the Surface Pressure Spectra between NACA 65-410 and NACA 0012

An important aspect of the present study is to compare the post-stall surface pressure fluctuation spectra between the symmetric NACA 0012 airfoil and the cambered NACA 65-410 airfoil, where both experiments were carried out in the same test section and with similar airfoil parameters (i.e., chord length and aspect ratio) and flow conditions (i.e., Reynolds number and free-stream turbulence level). As such, the comparison highlights the distinctive stall dynamics of the two airfoil profiles.

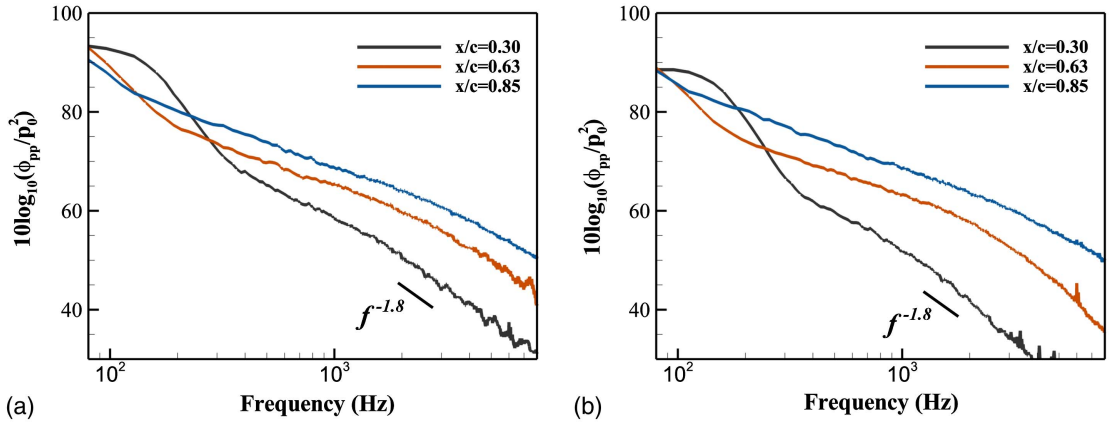

Fig. 7. Power spectral density of the unsteady surface pressure fluctuations of the NACA 0012 airfoil at post-stall angles of attack of (a) $\alpha = 15°$; and (b) $\alpha = 18°$ for comparison with the present NACA 65-410 under similar flow conditions.

Fig. 7 shows the surface pressure fluctuation spectra of the NACA 0012 airfoil at two angles of attack of $\alpha = 15°$ and 18°, respectively, corresponding to the full- and deep-stall conditions of the NACA 65-410. It should be mentioned that because the aerodynamic loading on the NACA 65-410 is constantly higher than that of the NACA 0012 even after full stall, the two angles of attack from the NACA 0012 were chosen such that they represent immediately after stall (15°) and well into stall (18°) conditions, respectively, similar to the NACA 65-410 stall conditions. Three chordwise measurement locations of $x/c = 0.3$, 0.63, and 0.85 were chosen to be close to those presented for the NACA 65-410 in Fig. 6. The overall dynamics of the surface pressure fluctuations resemble those of the cambered airfoil, with mostly monotonic decrease with approximately $f^{-1.8}$ gradient across the range of frequencies investigated. However, there are two notable differences between the symmetric and cambered airfoils. Firstly, there is a spectral hump at low frequencies ($f \leq 300$ Hz) for the chordwise locations of $x/c = 0.3$, which may be associated with distinct flow features of the NACA 0012 airfoil during stall. Note that the surface pressure spectra of the NACA 65-410 at $x/c = 0.3$ are not presented here for the sake of brevity; however, the result does not show a clear spectral hump at similar frequencies. Secondly, and more importantly, as briefly discussed in the earlier section, the magnitude variation of the surface pressure fluctuation spectra of the NACA 0012 airfoil from leading edge to trailing edge is considerably more significant than those of the NACA 65-410 airfoil (refer to Fig. 6). Moreover, the PSD magnitude increases with increasing downstream distance, which is a direct contrast to the NACA 65-410 airfoil results. For the NACA 65-410, the PSD magnitude drops slightly across the frequency range as the measurement location moves downstream toward the trailing edge. This observation is consistent with the measurements performed by Bertagnolio et al. (2015) for their NACA 0015 and NACA 63-418 airfoils at much higher Reynolds numbers. Their NACA 0015 airfoil exhibits a notable increase in the PSD magnitude of the surface pressure fluctuations from the leading edge to the midchord, whereas the magnitude remains comparable for NACA 63-418 from midchord to the trailing edge. The dynamics of the changes in surface pressure spectra are yet to be fully understood, but they point to the fact that scaling of the surface pressure fluctuation spectra may take different forms for different airfoils.

Characteristics of the Turbulent Structures

To investigate the characteristics of the turbulent structures associated with the surface pressure fluctuations, autocorrelation and cross-correlation analyses of the surface pressure fluctuation signals were performed using both the streamwise and spanwise dynamic transducers. The autocorrelation provides an indication of the frequency of the most energetic turbulent structure exerting on the measurement location, and cross-correlation analysis allows an evaluation of the correlation length scales of the structures.

Fig. 8 shows the distribution of autocorrelation coefficients in the time domain, $R_{pp}(\tau)$, and the corresponding ϕ_{pp} in the frequency domain of the unsteady surface pressure fluctuations for the chordwise locations of $x/c = 0.23, 0.55$, and 0.88 at the four angles of attack. The autocorrelation results represent the evolution of the turbulent structures from the leading edge to the trailing edge of the airfoil in the pre- and post-stall conditions. The normalized autocorrelation coefficients in the time domain are determined as follows (Palumbo 2012):

$$R_{pp}(\tau) = \frac{\overline{p'(t)p'(t-\tau)}}{{p'_{rms}}^2} \tag{1}$$

where the prime = fluctuating part of the quantity; and *rms* = root-mean-square operation. The decay gradient and the time lag, τ, of the coefficient distribution can provide useful information of the scale of the dominant turbulent structures. Moreover, its frequency domain power spectral density ϕ_{pp} can then be determined by applying fast Fourier transform to the autocorrelation function, which identifies the prominent frequencies associated with the flow structures. Note that here, unlike in the previous section on unsteady surface pressure results, ϕ_{pp} is normalized with the respective maximum magnitude, i.e., $\phi_{pp}/\phi_{pp,\max}$, to show the frequencies peaks more clearly. As can be observed in Fig. 8, the frequencies associated with the turbulent structures decrease continuously as the angle of attack increases from $\alpha = 7°$ pre-stall to $\alpha = 15°$ post-stall, regardless of the measurement location. Moreover, there exists a marked difference between near-stall and post-stall conditions. When the airfoil is at full stall $\alpha \geq 13°$, the autocorrelation coefficient function, $R_{pp}(\tau)$, widens considerably, suggesting that the surface pressure fluctuations are primarily influenced by the large-scale turbulent vortices, corresponding to low-frequency energy contents present in the separated shear layers, which are responsible for the stall noise. A deeper stall leads to noticeably larger turbulent structure, and therefore an increase of stall noise at even lower frequencies. When the measurement location moves downstream, the autocorrelation peak associated with the dominant flow structures shifts to lower frequencies, for instance, comparing $\alpha = 13°$ from Figs. 8(d–f). This is expected, as the turbulent structures grow in size as they convect downstream in the separated

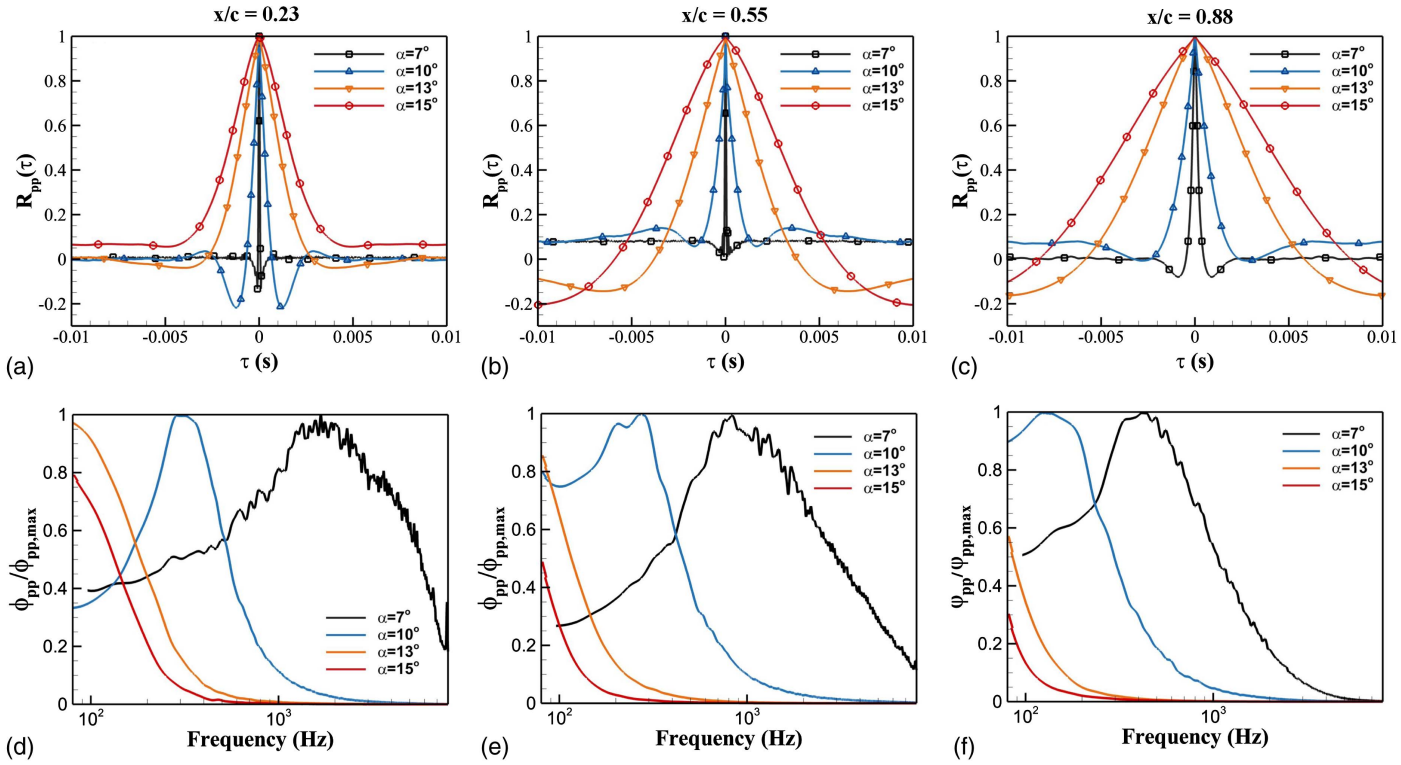

Fig. 8. Autocorrelation of the unsteady surface pressure spectra of the NACA 65-410 at angles of attack of $\alpha = 7°$, 10°, 13°, and 15°. The time-domain coefficients $R_{pp}(\tau)$ are shown for the chordwise locations of (a) $x/c = 0.23$; (b) $x/c = 0.55$; and (c) $x/c = 0.88$; and the corresponding normalized frequency domain power spectral densities, $\phi_{pp}/\phi_{pp,\max}$, are shown for the chordwise locations of (d) $x/c = 0.23$; (e) $x/c = 0.55$; and (f) $x/c = 0.88$.

flow. However, it should be remarked that this growth of the boundary layer is physically different from flow separation and stall. At a near-stall angle of attack of $\alpha = 10°$, the autocorrelation function exhibits some distinct changes when the measurement location moves from the leading edge to the trailing edge of the airfoil, see Figs. 8(a–c), possibly due to the dynamic flow development between attached and separated states.

According to the BPM model (Brooks et al. 1989) and an earlier study by Moreau et al. (2009), the size and associated frequency of the turbulent structures along the spanwise directions are equally crucial in understanding and modeling of airfoil separation and stall noise. With spanwise dynamic transducers at several chordwise locations toward the trailing edge, the spanwise correlation length, $\Lambda(f)$, can be determined as (Maryami et al. 2019, 2020)

$$\Lambda(f) = \int_0^\infty \gamma(f, \eta_z) d\Delta z \tag{2}$$

where the coherence between two surface pressure signals, $\gamma(f, \eta_z)$, is defined as

$$\gamma^2(f, \eta_z) = \frac{|\phi_{p_m,p_n}(f, \eta_z)|^2}{\phi_{p_m,p_m}(f, \eta_z)\phi_{p_n,p_n}(f, \eta_z)} \tag{3}$$

Here, η_z = spanwise location of the measurement in the z-direction. Due to a limited number of spanwise transducers, a summation of the coherence between each pair of transducers will be largely inaccurate. Hence, in practice, the calculated coherence $\gamma(f, \eta_z)$ between each transducer pair is fitted through an exponential function, which then is substituted into Eq. (2) to determine the spanwise correlation length, $\Lambda(f)$ (Palumbo 2012). The exponential function can be written as

$$\gamma(f, \eta_{z,0}, \eta_{z,i}) = e^{\frac{|\eta_{z,0} - \eta_{z,i}|}{L_c(f)}}, \qquad i = 1, 2, 3 \ldots \tag{4}$$

where $|\eta_{z,0} - \eta_{z,i}|$ = distance between a pair of spanwise microphones; and $L_c(f)$ = frequency-dependent length computed for the best exponential fit. Under the present experimental conditions, the uncertainty of the spanwise length scale is estimated to be 7% based on the primary uncertainty of the dynamic transducer and the exponential fit at 95% confidence interval (Bendat and Piersol 2011; Palumbo 2012).

Fig. 9 shows the correlation length, normalized by the airfoil chord c, for two chordwise locations of $x/c = 0.72$ and 0.88. The correlation length at low frequencies ($f \approx 50$ Hz) increases by almost an order of magnitude at post-stall conditions, compared with the pre-stall angles. Between the two post-stall cases, the length scale almost doubles when the angle of attack increases from $\alpha = 13°$ to 15°. Nevertheless, both length scales decrease rapidly and converge to their pre-stall counterparts after approximately $f = 150$ Hz. At even higher frequencies of $f \geq 200$ Hz, the spanwise length scales of the associated turbulent structures at $\alpha = 10°$ surpasses those at post-stall angles. Furthermore, moving from $x/c = 0.72$ to 0.88, the spanwise length scales experience further growth except at $\alpha = 15°$, where a slight decrease is observed. Results from the spanwise turbulent length scales correspond well with those from the autocorrelation analysis, because at post-stall conditions, the flow dynamics are primarily governed by the low-frequency energy contents associated with the large-scale turbulent structures. From the spanwise length scale results, the spanwise scale of the turbulent structures of the fully stalled NACA 65-410 can be as large as approximately half of the airfoil chord, i.e., $0.45c$.

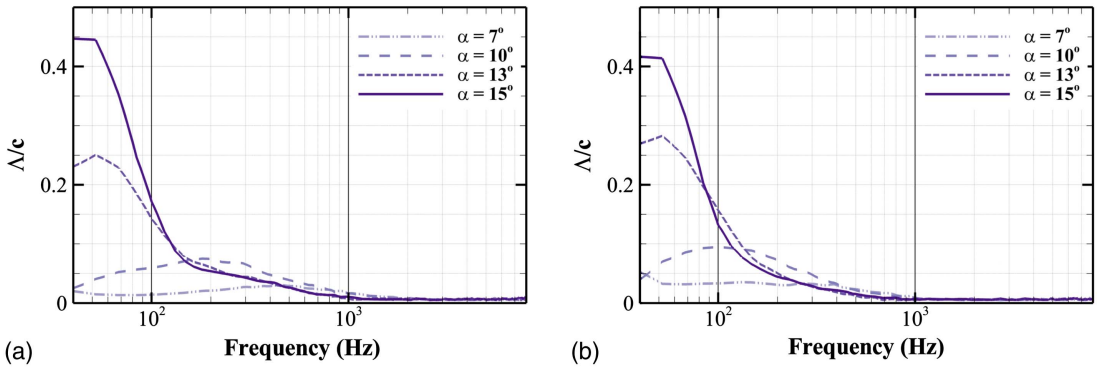

Fig. 9. Spanwise correlation length Λ, as determined from Eq. (2) and normalized by chord c, at the angles of attack of $\alpha = 7°$, 10°, 13°, and 15° for the chordwise locations of (a) $x/c = 0.72$; and (b) $x/c = 0.88$.

Scaling of the Surface Pressure Spectra

In the stall noise model proposed by Moreau et al. (2009) from their combined experimental and numerical studies, the surface pressure spectra can be approximately scaled with U_∞^3, based on a NACA 0012 airfoil at angles of attack of $\alpha = 16°$ and 18°. Bertagnolio et al. (2015, 2017) later attempted to scale the surface pressure fluctuation spectra for their stall noise model. Based on the relatively linear relationship between the downstream distance and the unsteady surface pressure spectra, they argued that the scaling should be proportional to $\sim lU_\infty^3$, where l is the characteristic length associated with the stall dynamics. Subsequently, the unsteady surface pressure spectra can be scaled as (Bertagnolio et al. 2017)

$$\phi_{pp,l} = \phi_{pp}/[q^2 \cdot (l/U_\infty)] \tag{5}$$

where $\phi_{pp,l}$ = power spectral density of the unsteady surface pressure fluctuation normalized by the characteristic length l and the dynamic pressure of the free stream, $q = 0.5\rho U_\infty^2$. Moreover, the characteristic length l can be taken as the length from the flow separation point to the measurement location. As the airfoil is fully stalled, l can be reasonably taken as d_{xi}, where d_{xi} is the distance of the ith transducer to the leading edge, with sufficient accuracy (Bertagnolio et al. 2015). This can be clearly seen for the NACA 65-410 airfoil from both the relatively flat static pressure coefficient and the monotonically decreasing unsteady surface pressure spectra along the airfoil chord as the flow separates from the leading edge.

Figs. 10 and 11 show the scaled surface pressure fluctuation spectra plotted against the characteristic Strouhal number, $St_l = fl/U_\infty$, for the NACA 65-410 airfoil at the two free-stream velocities of $U_\infty = 20$ ms^{-1} and 30 ms^{-1} for the post-stall angles of attack of $\alpha = 13°$ and 15°. The additional experiments at $U_\infty = 30$ ms^{-1} were performed to examine the influence of the velocity variable U_∞ on the scaling approach. It can be observed that the unsteady surface pressure spectra along the airfoil chord collapse relatively well for both free-stream velocities, which reaffirms the effectiveness of the scaling approach at the present range of Reynolds numbers for the NACA 65-410 profile. However, there exist noticeable discrepancies for the measurement locations close to the leading edge, which could suggest that a separate scaling or an additional length scale factor should be considered for the leading-edge measurements, likely due to their close distance to the flow separation point and hence enduring different flow effects. Moreover, at near-stall conditions, it is often difficult to accurately identify the flow separation point, and hence, a different approach may be considered for airfoils that are yet to be fully stalled from the leading edge.

Conclusions

At high angles of attack, an airfoil experiences stall with elevated self-noise levels, known as stall noise. The present study experimentally investigated the near-field aeroacoustic characteristics

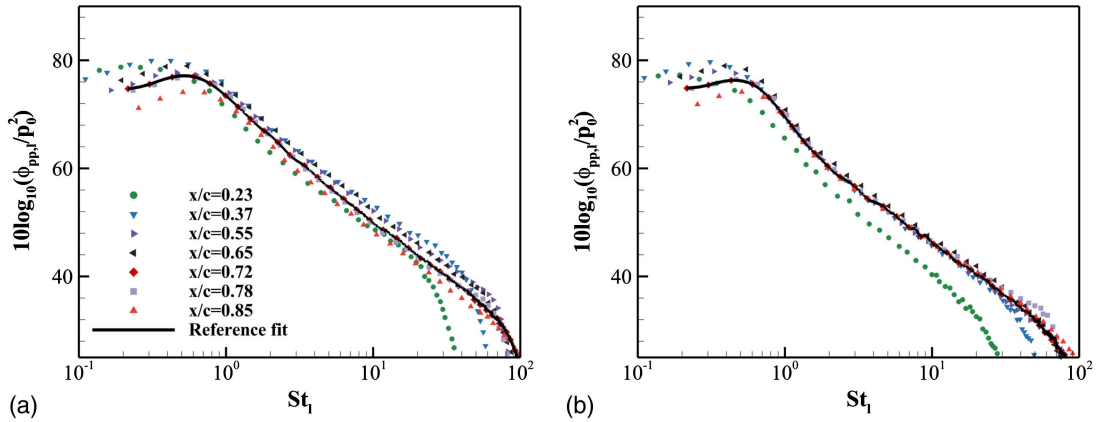

Fig. 10. Scaling of the unsteady surface pressure spectra $[\sim 1/(lU_\infty^3)]$ of the NACA 65-410 at post-stall angles of attack of (a) $\alpha = 13°$; and (b) $\alpha = 15°$ and free-stream velocity of $U_\infty = 20$ ms^{-1}.

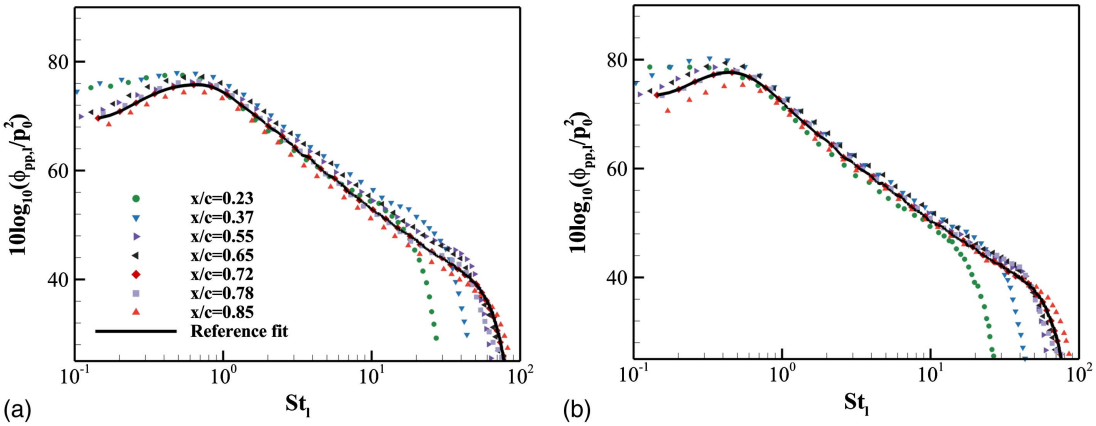

Fig. 11. Scaling of the unsteady surface pressure spectra [$\sim 1/(lU_\infty^3)$] of the NACA 65-410 at post-stall angles of attack of (a) $\alpha = 13°$; and (b) $\alpha = 15°$ and free-stream velocity of $U_\infty = 30$ ms^{-1}.

of a cambered NACA 65-410 airfoil from pre- to post-stall conditions, and compared the stall behavior with that obtained from a symmetric NACA 0012 airfoil at similar test conditions. By varying the geometric angles of attack from $\alpha = 7°$ to 15° at a moderate Reynolds number, changes in the surface pressure fluctuations from pre-stall to partial separation and then full stall were recorded, with pressure transducers distributed along both the streamwise and spanwise directions. The surface pressure fluctuations, pressure autocorrelation function, and spanwise correlation length results showed that the near-field dynamics of the stalled NACA 65-410 are primarily dominated by turbulent structures at low frequencies. This effect was even more pronounced when the airfoil enters deep stall. On the other hand, at near-stall conditions, the airfoil displayed notable variations in the surface pressure spectra along the chord and its frequency energy content associated with the turbulent structures.

Comparison with the symmetric NACA 0012 airfoil showed some marked differences in the stall behavior between the two airfoils. For instance, the PSD magnitude of the surface pressure spectra of NACA 0012 varied more significantly from the leading edge to the trailing edge during full stall. More importantly, the PSD magnitude increases with increasing downstream distance for the NACA 0012, opposite to that of the NACA 65-410. By defining the characteristic length of the stalled airfoil, the scaling approach proposed by Bertagnolio et al. (2017) has been applied to the surface pressure spectra of the NACA 65-410 airfoil at post-stall conditions. The results showed that the unsteady surface pressure can be scaled effectively except at locations close to the leading edge. Nevertheless, further studies of the scaling laws for the transition range of angle of attack, where partial separation occurs, are necessary.

Data Availability Statement

Some or all data, models, or code that support the findings of this study are available from the corresponding author upon reasonable request.

Acknowledgments

The authors would like to acknowledge the financial support from Engineering and Physical Sciences Research Council (EPSRC) for the present study via research Grant No. EP/R010846/1 and the second author would like to also acknowledge the support from EPSRC DTP scholarship.

References

Afshari, A., M. Azarpeyvand, A. A. Dehghan, M. Szöke, and R. Maryami. 2019. "Trailing-edge flow manipulation using streamwise finlets." *J. Fluid Mech.* 870 (Jul): 617–650. https://doi.org/10.1017/jfm.2019.249.

Bendat, J. S., and A. G. Piersol. 2011. *Random data: Analysis and measurement procedures*. Hoboken, NJ: Wiley.

Bertagnolio, F., H. A. Madsen, A. Fischer, and C. Bak. 2015. "Experimental characterization of stall noise—Toward its modelling." In *Proc., 6th Int. Conf. on Wind Turbine Noise*. Reston, VA: AIAA.

Bertagnolio, F., H. A. Madsen, A. Fischer, and C. Bak. 2017. "A semi-empirical airfoil stall noise model based on surface pressure measurements." *J. Sound Vib.* 387 (Jan): 127–162. https://doi.org/10.1016/j.jsv.2016.09.033.

Brooks, T. F., D. S. Pope, and M. A. Marcolini. 1989. *Airfoil self-noise and prediction.* Rep. No. NASA-RP-1218. Hampton, VA: NASA Langley Research Center.

Drela, M. 1989. "XFOIL: An analysis and design system for low Reynolds number airfoils." In Vol. 54 of *Low Reynolds number aerodynamics. lecture notes in engineering*, edited by T. J. Mueller Berlin: Springer. https://doi.org/10.1007/978-3-642-84010-4_1.

Garcia-Sagrado, A. 2008. "Boundary layer and trailing-edge noise source." Ph.D. thesis, Dept. of Engineering, Univ. of Cambridge.

Gault, D. E. 1957. *A correlation of low-speed, airfoil-section stalling characteristics with Reynolds number and airfoil geometry.* Rep. No. NASA TN-3963. Moffet Field, CA: Ames Aeronautical Laboratory.

Jarup, L., et al. 2005. "Hypertension and exposure to noise near airports (HYENA): Study design and noise exposure assessment." *Environ. Health Perspect.* 113 (11): 1473–1478. https://doi.org/10.1289/ehp.8037.

Jones, B. M. 1934. "Stalling." *Aeronaut. J.* 38 (285): 753–770. https://doi.org/10.1017/S0368393100109782.

Kocheemoolayil, J. G., and S. K. Lele. 2016. "Large eddy simulation of airfoil self-noise at high Reynolds number." In *Proc., 22nd AIAA/CEAS Aeroacoustics Conf.* Reston, VA: AIAA.

Kurtz, D. W., and J. E. Marte. 1970. *A review of aerodynamic noise from propellers, rotors, and lift fans*. Rep. No. NASA TR-32-1462. Pasadena, CA: California Institute of Technology.

Lyon, C. A., M. S. Selig, and A. P. Broeren. 1997. "Boundary layer trips on airfoils at low Reynolds numbers." In *Proc., 35th Aerospace Sciences Meeting and Exhibit.* Reston, VA: AIAA.

Maryami, R., M. Azarpeyvand, A. A. Dehghan, and A. Afshari. 2019. "An experimental investigation of the surface pressure fluctuations for

round cylinders." *J Fluids Eng* 141 (6): 1285. https://doi.org/10.1115/1.4042036.

Maryami, R., S. A. Showkat Ali, M. Azarpeyvand, and A. Afshari. 2020. "Turbulent flow interaction with a circular cylinder." *Phys. Fluids* 32 (1): 015105. https://doi.org/10.1063/1.5119967.

Mayer, Y. D., H. Kamliya Jawahar, M. Szöke, S. A. Showkat Ali, and M. Azarpeyvand. 2019a. "Design and performance of an aeroacoustic wind tunnel facility at the University of Bristol." *Appl. Acoust*. 155 (Dec): 358–370. https://doi.org/10.1016/j.apacoust.2019.06.005.

Mayer, Y. D., B. Zang, and M. Azarpeyvand. 2019b. "Aeroacoustic characteristics of a NACA 0012 airfoil for attached and stalled flow conditions." In *Proc., 25th AIAA/CEAS Aeroacoustics Conf.* Reston, VA: AIAA.

Mayer, Y. D., B. Zang, and M. Azarpeyvand. 2020. "Aeroacoustic investigation of an oscillating airfoil in the pre- and post-stall regime." *Aerosp. Sci. Technol.* 103 (Aug): 105880. https://doi.org/10.1016/j.ast.2020.105880.

Mccullough, G. B., and D. E. Gault. 1951. *Examples of three representative types of airfoil-section stall at low speed*. Rep. No. NASA TN-2502. Moffet Field, CA: Ames Aeronautical Laboratory.

Mish, P. F. 2003. "An experimental investigation of unsteady surface pressure on single and multiple airfoils." Ph.D. thesis, Dept. of Aerospace and Ocean Engineering, Virginia Polytechnic Institute and State Univ.

Moreau, S., J. Christophe, and M. Roger. 2008. "LES of the trailing-edge flow and noise of a NACA 0012 airfoil near stall." In *Proc., Summer Program*. Stanford, CA: Stanford Univ.

Moreau, S., M. Roger, and J. Christophe. 2009. "Flow features and self-noise of airfoils near stall or in stall." In *Proc., 15th AIAA/CEAS Aeroacoustics Conf.* Reston, VA: AIAA.

Nobbs, B., C. J. Doolan, and D. J. Moreau. 2012. "Characterisation of noise in house affected by wind turbine noise." In *Proc., Acoustics 2012*. Canberra, Australia: Australian Acoustical Society.

Palumbo, D. 2012. "Determining correlation and coherence lengths in turbulent boundary layer flight data." *J. Sound Vib.* 331 (16): 3721–3737. https://doi.org/10.1016/j.jsv.2012.03.015.

Petrilli, J. L., R. C. Paul, A. Gopalarathnam, and N. T. Frink. 2013. "A CFD database for airfoils and wings at post-stall angles of attack." In *Proc., 31st AIAA Applied Aerodynamics Conf.* Reston, VA: American Institute of Aeronautics and Astronautics.

Reilly, D. N. 1967. "A useful method of airfoil stall prediction." *J. Aircr.* 4 (6): 567–568. https://doi.org/10.2514/3.59413.

Schuele, C. Y., and K.-S. S. Rossignol. 2013. "Trailing-edge noise modeling and validation for separated flow conditions." In *Proc., 19th AIAA/CEAS Aeroacoustics Conf.* Reston, VA: AIAA.

Szöke, M. 2019. "Trailing edge noise control using active flow control methods." Ph.D. thesis, Dept. of Aerospace Engineering, Univ. of Bristol.

Turner, J. M., and J. W. Kim. 2020a. "Aerofoil dipole noise due to flow separation and stall at a low Reynolds number." *Int. J. Heat Fluid Flow* 86 (Dec): 108715. https://doi.org/10.1016/j.ijheatfluidflow.2020.108715.

Turner, J. M., and J. W. Kim. 2020b. "Effect of spanwise domain size on direct numerical simulations of airfoil noise during flow separation and stall." *Phys. Fluids* 32 (6): 065103. https://doi.org/10.1063/5.0009664.

Vemuri, S. S., X. Liu, B. Zang, and M. Azarpeyvand. 2020. "On the use of leading-edge serrations for noise control in a tandem airfoil configuration." *Phys Fluids* 32 (7): 077102. https://doi.org/10.1063/5.0012958.

Welch, P. 1967. "The use of fast Fourier transform for the estimation of power spectra: A method based on time averaging over short, modified periodograms." *IEEE Trans. Audio Electroacoust.* 15 (2): 70–73. https://doi.org/10.1109/TAU.1967.1161901.

Westphal, W. R., and W. R. Godwin. 1951. *Comparison of NACA 65-series compressor-blade pressure distributions and performance in a rotor and in cascade*. Hampton, VA: Langley Aeronautical Laboratory.

Wolf, W. R., and S. K. Lele. 2012. "Trailing-edge noise prediction using compressible large eddy simulation and acoustic analogy." *AIAA J.* 50 (11): 2423–2434. https://doi.org/10.2514/1.J051638.